Journal of Materials Chemistry C

ROYAL SOCIETY OF CHEMISTRY

PAPER

View Article Online
View Journal | View Issue

Cite this: J. Mater. Chem. C, 2020, 8, 9707

Mode cleaning in graphene oxide-doped polymeric whispering gallery mode microresonators

Nathália B. Tomazio, [a] Kelly T. Paula,[a] Franciele R. Henrique,[a] Marcelo B. Andrade, [a] Xavier Roselló-Mechó,[b] Martina Delgado-Pinar,[b] Miguel V. Andrés[b] and Cleber R. Mendonca*[a]

Received 19th May 2020,
Accepted 21st June 2020

DOI: 10.1039/d0tc02403a

rsc.li/materials-c

The strategy to incorporate graphene oxide (GO) in a composite material offers significant opportunities to realize compact photonic devices, such as saturable absorbers and polarization selective devices. However, the processing of GO-based composites by direct laser writing, which would afford vast patterning and material flexibility in a single step process, has been little addressed. In this work, we investigated the mechanisms underlying a mode cleaning effect in polymeric whispering gallery mode microresonators containing GO, aiming at the development of on-chip integrable photonic devices. We fabricated the microresonators (cavity loaded Q-factor of 20 000 at 1550 nm) in a single step of femtosecond laser writing *via* two-photon polymerization. By calculating the resonance response to damping mechanisms in the microresonators, we showed that additional losses introduced by GO play a major role in reducing the visibility of a number of resonances up to the point of effectively filtering a set of modes out. Interestingly, although the presence of GO leads to extra losses in the microresonator, it does not change the order of magnitude of the Q-factor of the highest extinction ratio resonances. Overall, this work offers interesting physical insights that can be useful for the design and fabrication of GO-based photonic micro/nanodevices.

Introduction

Graphene Oxide (GO) is chemically modified graphene[1] containing oxygen functional groups, such as epoxides, alcohols and carboxylic acids on the basal plane and/or on the sheet edge.[2] It has become a highly promising member of the graphene family due to its intriguing physical and chemical properties arising from the hybridization of the sp^2- and sp^3-carbon atoms.[1–3] The manipulation of the relative fraction of the sp^2-hybridized domains of GO by either chemical or laser irradiation methods provides opportunities for tailoring its optical and electrical properties, such as conductivity, bandgap and refractive index.[4,5] Moreover, the presence of oxygen-functional groups allows GO to interact with a myriad of organic and inorganic materials in non-covalent, covalent and ionic manners.[5] This makes GO easier to process and more soluble compared to graphene, which ultimately translates into lower-cost manufacturing and easier integration into a range of photonic systems.

An efficient way to harness these properties for the development of photonic devices is to incorporate GO in a composite material.[6] Besides leveraging on the outstanding properties of GO, this strategy confers practical advantages, such as flexible packaging and on-chip integration.[6,7] GO-based composites have been used for a wide range of applications, including ultrafast lasers,[7,8] polarization selective devices[9] and multimode optical recording,[10] and have been mostly patterned by 2D techniques. Nevertheless, the processing of GO-based composites by direct laser writing, which affords vast patterning and material flexibility in a single step process, has been far less explored.

In this work, we investigate the mechanisms underlying a mode cleaning observed in GO-doped whispering gallery mode (WGM) microresonators fabricated by femtosecond laser writing *via* two-photon polymerization (2PP) using an acrylic-based photoresist doped with GO. The favorable properties of WGM microresonators, such as high-Q, tight mode confinement and frequency selectivity, make them a compelling platform for fundamental studies in quantum electrodynamics and nonlinear optics and for applications ranging from optical switches

[a] São Carlos Institute of Physics, University of São Paulo, PO Box 369, 13560-970, São Carlos, SP, Brazil. E-mail: crmendon@ifsc.usp.br
[b] Department of Applied Physics and Electromagnetism – ICMUV, University of Valencia, 46100, Valencia, Spain

in photonic circuits to biosensors.[11–17] In our experiments, light was coupled to the WGM microresonators *via* evanescent field through the use of tapered optical fibers. The mode cleaning was investigated by modeling the resonances with the transmission function of a straight waveguide coupled to a microresonator, which takes into account the main mechanisms of power dissipation of this system. The extra absorption and scattering introduced by GO were quantified through modeling of absorbance data obtained with the help of near-infrared spectroscopy. In addition, the GO-doped WGM microresonators were characterized by scanning electron microscopy and by Raman spectroscopy.

Results and discussion

Graphene oxide-doped whispering gallery mode microresonators

Fig. 1a shows a typical GO-doped WGM microresonator fabricated by employing 0.1 nJ pulses from a Ti:sapphire oscillator with 40 μm s^{-1} of laser scan speed. The hollow microcylinders exhibit an outer diameter of 53 μm, 6.5 μm of sidewall thickness and approximately 150 μm of height. They feature good structural integrity and smooth sidewalls, despite the presence of GO, and low shrinkage.

Surface Enhanced Raman Spectroscopy (SERS), performed by coating the microresonators with a gold nanoscale layer, confirmed the presence of GO in the microstructures.[18–20] The measurement was taken in a LabRAM HR micro Raman system using 6 mW of a solid-state laser centered at 532 nm. Fig. 1b shows the Raman spectra of an undoped and a GO-doped microresonator. The GO-doped microresonator spectrum differs from that of its undoped counterpart by two prominent peaks (at 1329 cm^{-1} and 1580 cm^{-1}), arising from vibrations of the sp^2 carbon of GO.[21] The D band at 1329 cm^{-1} is due to the breathing mode of the aromatic rings,[22] whereas the G band at 1580 cm^{-1} corresponds to the first-order scattering of the E_{2g} mode.[21] The other peaks at 1280, 1410, 1455, 1637 and 1736 cm^{-1} are assigned to the =CH rock, the deformation vibrations of CH_2,[23] the vibration of the photoinitiator aromatic ring[24] and the stretching of the carbon–carbon double bond (C=C) and the carbonyl group (C=O) of the monomers, respectively.[25–27]

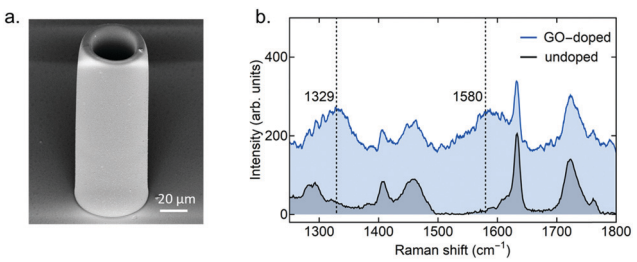

Fig. 1 (a) Scanning electron micrograph of a typical graphene oxide-doped microresonator fabricated by femtosecond laser writing *via* two-photon polymerization. (b) Raman spectra of an undoped (gray) and a GO-doped (blue) microresonator. Highlighted in the graph is the spectral position of the two peaks that indicate the presence of graphene oxide.

Light coupling to the graphene oxide-doped microresonators

Fig. 2b displays the set of whispering gallery modes for independent polarization states of a GO-doped microresonator in the range of 1520 to 1540 nm, excited in the undercoupling regime through a 2 μm-waist taper. Consecutive azimuthal modes could be easily identified in the spectrum, and their corresponding free spectral range (FSR) was found to be around 9.2 nm, in agreement with the expected value for these microresonators at this wavelength window (FSR = 9.34 nm at 1.53 μm). The theoretical FSR was calculated through:[12,15]

$$\mathrm{FSR} = \frac{\lambda^2}{2\pi a n} \quad (1)$$

in which, λ is the wavelength of light, and a and n are the microresonator's radius and refractive index, respectively. The highest extinction ratio resonance is 6.2 dB deep and exhibits a Q-factor of 1.1×10^4 (Fig. 2b). An asymmetric Lorentzian fit was used to determine its linewidth.[28,29] For comparison purposes, the resonance spectrum of an undoped microresonator with the same dimensions of its GO-doped counterpart is shown in Fig. 2c. It was interrogated with the same taper and coupling conditions as those employed to load the GO-doped microresonator whose resonance spectrum is shown in Fig. 2b.

The undoped microresonator spectrum is filled with resonances featuring a range of extinction ratios and linewidths, regardless of the coupled power. On the other hand, notably fewer resonances were systematically observed for the GO-doped microresonators, which places the presence of GO as the determinant factor in reducing the visibility of a number of resonances up to the point of effectively filtering (cleaning out) a set of modes. Interestingly, even though the presence of GO brings up extra losses to the microresonator, the Q-factor of the highest extinction ratio resonances does not decrease significantly. As can be seen in Fig. 2b and c, the linewidth of the highest extinction ratio resonance of the GO-doped microresonator spectrum is only 1.3 times broader than a resonance with similar characteristics in the undoped microresonator spectrum, which does not change the order of magnitude of the Q-factor.

It is important to notice that the mode cleaning occurs for both polarizations. This result is consistent with our hypothesis that polarization-selective effects do not play a role in extinguishing certain modes. Since the GO flakes are randomly oriented throughout the microresonators, we expected any polarization-dependent effect to be averaged out along propagation.

The overall change in the resonance spectrum with the incorporation of GO was investigated by modeling the resonances with the transmission function of a straight waveguide coupled to a resonator. The transmission response of the system at the frequency ω is given by:[11,30]

$$T(\omega) = T_0 \frac{(\omega-\omega_0)^2 + \left(\frac{1}{\tau_0} - \frac{1}{\tau_c}\right)^2}{(\omega-\omega_0)^2 + \left(\frac{\Delta\omega}{2}\right)^2} \quad (2)$$

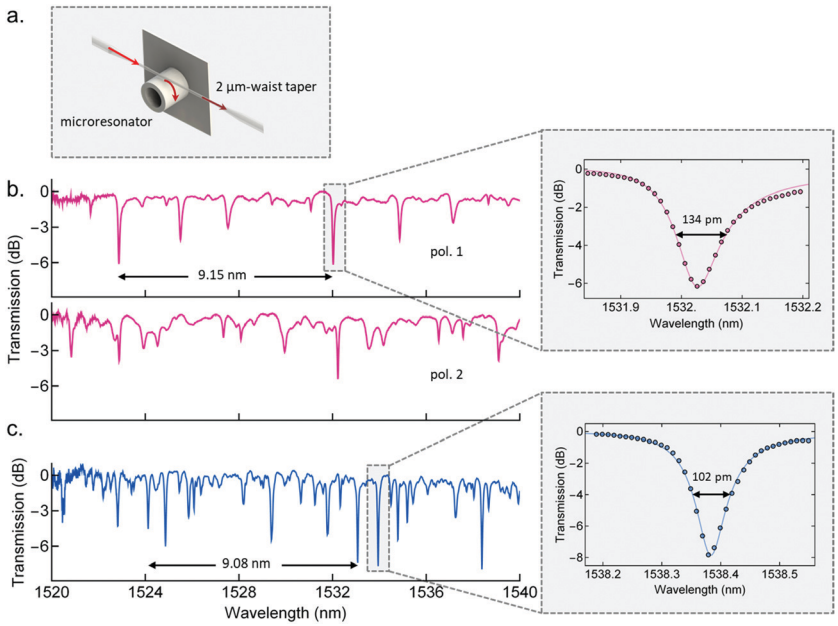

Fig. 2 (a) Schematics of the evanescent field-based coupling of light to the microresonators through the use of tapered fibers. (b and c) Transmission spectra of a 2 μm-waist taper coupled to a (b) GO-doped microresonator for different polarization states (750 μW of input power) and to an (c) undoped microresonator (35 μW of input power). Shown in the right-hand side are the highest extinction ratio resonances for a GO-doped (above) and for an undoped (below) microresonator. The free spectral range for both spectra is highlighted in the graphs.

which includes a sigmoid function to capture the asymmetry of the resonances:[28]

$$\Delta\omega = \frac{4\left(\frac{1}{\tau_0}+\frac{1}{\tau_c}\right)}{1+\exp[a(\omega-\omega_0)]} \quad (3)$$

In the eqn (2) and (3), T_0 is an offset correction factor, ω_0 is the resonance frequency, a is the asymmetry factor and τ_0 and τ_c are the lifetimes associated with power dissipation through intrinsic losses in the microresonator and through coupling losses, respectively.

The decay rate due to intrinsic losses (τ_0) is proportional to the intrinsic Q-factor (Q_{in}):[30]

$$\tau_0 = \frac{2Q_{in}}{\omega_0} \quad (4)$$

Q_{in} accounts for the main sources of loss in the microresonators, which are material attenuation (material absorption and scattering in the volume) and surface scattering at the resonator sidewalls. Due to the large diameter of the microresonators compared to wavelength of light, radiation losses can be neglected in this particular case. Q_{in} can be discriminated into the Q-factors associated with material attenuation (Q_{mat}) and surface scattering ($Q_{s.s.}$) according to:[11]

$$\frac{1}{Q_{in}} = \frac{1}{Q_{mat}} + \frac{1}{Q_{s.s}} \quad (5)$$

Note that the material attenuation (Q_{mat}) and the surface scattering contribution to the Q-factor ($Q_{s.s.}$) ultimately affect the photon lifetime associated with intrinsic losses (τ_0), whose variation leads to a different transmission response for a given resonance.

The contribution of material attenuation to the intrinsic Q-factor can be determined through:[11]

$$Q_{mat} = \frac{2\pi n}{\lambda_0 \alpha} \quad (6)$$

where n, λ_0 and α denote the refractive index, the resonance wavelength and the material attenuation coefficient, respectively.

The impact of the incorporation of GO on each resonance's linewidth and extinction ratio was therefore evaluated through the variation of its transmission curve in response to an increase of intrinsic losses. We adjusted the material attenuation and the surface scattering contribution to the Q-factor of each individual resonance to match both Q_{mat} and the $Q_{s.s.}$ that are expected with the incorporation of GO to the microresonator. The latter was obtained by comparing each resonance of the undoped microresonator to the resonances of the GO-doped microresonator's spectrum to find the best match in terms of linewidth and extinction ratio. The $Q_{s.s.}$ of the undoped resonance was then adjusted according to the $Q_{s.s.}$ of its best matched GO-doped resonance. For example, the undoped resonance tagged in Fig. 2c, which exhibits 8 dB of extinction ratio and 102 pm of linewidth, had its surface scattering Q-factor decreased from 23 900 to 19 840 to match the $Q_{s.s.}$ of the GO-doped resonance tagged in Fig. 2b (6.2 dB of extinction ratio and 134 pm of linewidth). All the undoped resonances had their material attenuation Q-factor (Q_{mat}) adjusted according to the increase of the material attenuation coefficient (α) from 0.32 cm^{-1} (undoped polymer) to 0.8 cm^{-1} (GO-doped polymer). Q_{mat} was calculated through eqn (6).

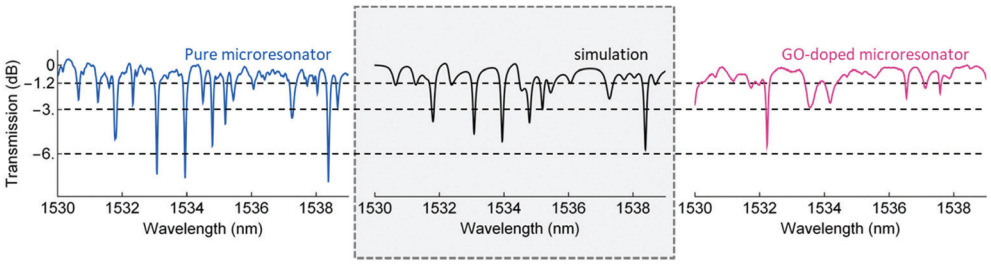

Fig. 3 From left to right: Resonance spectra (1530–1539 nm) for the undoped microresonator (experimental data), for the simulation and for the GO-doped microresonator (experimental data).

The material attenuation coefficient of the undoped (α_p) and the GO-doped polymer (α_{GO}) had been obtained through modeling of absorbance measurements as described in the Experimental section.

By modeling the experimental resonances for the undoped microresonator within a 10 nm-spectral range (blue spectrum on the left of Fig. 3) to simulate the incorporation of GO to the microresonator, we obtained the spectrum highlighted in Fig. 3 (black spectrum). The presence of GO broadens the linewidth of the resonances and decreases their extinction ratio to different extends. The resonances that are closest to the critical coupling condition, like the one tagged in Fig. 2c, suffer a subtle broadening of their linewidth and have their extinction ratio decreased a little down 6 dB. On the other hand, the lowest extinction ratio resonances, which stand for over 40% of the resonance spectrum, undergo a stronger linewidth broadening and are attenuated to extinction ratio values below 1.2 dB.

As can be seen in Fig. 3, the overall aspect of the simulated spectrum, which includes the additional losses introduced by GO, matches reasonably well the one of the GO-doped microresonator (magenta spectrum), *i.e.*, they exhibit a similar number of resonances and there is a good match between the individual characteristics (linewidth and extinction ratio) of the remaining resonances of both spectra. This result reveals that the increase in the overall losses introduced by GO is the determinant factor behind the mode cleaning.

It is important to point out that our analysis does not allow checking the effect of GO on each specific resonance. Even though the undoped and GO-doped microresonators were designed to have the same dimensions, their modes cannot be identified and the same resonance cannot be spotted in the different spectra due to a combination of factors: (i) the microresonators suffer from polymerization shrinkage, which was minimized with the photoresist composition but could not be completely eliminated. The shrinkage introduces a subtle conical shape to the microresonators, thus making their diameter to vary along their axis. (ii) The taper is not guaranteed to approach the microresonator at the same height in every coupling attempt, which brings further uncertainty in the determination of the resonator dimensions. These factors, combined with the drift of the resonances in response to external perturbations, make it difficult to carry out a more detailed analysis of the effect of GO on each specific resonance.

Further mode suppression can be caused by loss mechanisms not taken into account in the aforementioned model, such as the presence of GO agglomerates throughout the microresonator and nonlinear absorptive effects (*e.g.*, saturable absorption[31]). The presence of GO agglomerates in the interior of the resonators, close to their inner sidewall surface, can selectively introduce losses to the modes depending on their radial order. In other words, the higher-order radial WGMs, which overlap the most with the agglomerates, are more susceptible to scattering than the most fundamental WGM. The saturable absorption contribution of GO can also affect the modes differently, and, similarly to the agglomerates, it introduces higher losses to the higher-order radial WGMs. Since the intensity profile of higher-order radial WGMs is more spread out inside the resonator, their peak intensity might not be high enough to saturate absorption, thus rendering these modes attenuated. On the other hand, the higher peak intensity of the most fundamental WGM might allow it to achieve saturation, which ultimately leads to lower absorption losses.

In a previous work, we studied the contribution of GO saturable absorption by carrying out nonlinear measurements in the GO-doped polymer using the femtosecond Z-scan technique with excitation at 1550 nm and by modeling the photo-carrier dynamics with a two-level system in the transient regime.[32] By fitting the experimental data to the aforementioned model, we found the saturation intensity to be 500 MW cm^{-2}.[32] This is much higher than the peak-intensity circulating in a fundamental WGM of the GO-doped microresonator for a pump power on the milliwatt level, thus ruling out completely the contribution of GO saturable absorption to the mode cleaning. For example, the circulating peak-intensity for the resonance highlighted in Fig. 2b was found to be 0.12 MW cm^{-2}, which is at least three orders of magnitude lower than the intensity required to saturate the absorption of GO (500 MW cm^{-2}). To calculate the circulating peak-intensity for the resonance highlighted in Fig. 2b, the mode area was determined by considering a mode featuring lateral and vertical spot sizes of 2 and 5 μm, respectively, and the power enhancement (P_c/P_{in}) achieved in the resonator was calculated using the expression provided in ref. 33:[33]

$$P_c = \frac{P_{in}}{\tau}\frac{4\kappa_{coup}}{(\kappa_{coup}+\kappa_{in})^2} \quad (7)$$

In which P_{in}, τ, κ_{coup} and κ_{in} denote the input power, the photon round trip time in the microresonator and the rate of

coupling losses and of intrinsic losses, respectively. The parameters κ_{coup} and κ_{in} for an individual resonance can be obtained by fitting it to **e**qn (2).

The mode cleaning effect could be achieved by other strategies than which is presented in this work. For example, by decreasing the microresonator's diameter to a few microns, one can obtain a resonance spectrum with only the fundamental radial WGMs.[34] In this case, radiation losses are considerably raised for both the fundamental and higher-order radial WGMs, but the latter are the most affected ones. Another way of cleaning the resonance spectrum would be by reducing the sidewall thickness of the hollow microresonators to dimensions comparable to the wavelength of light.[34,35] Although this is the most loss-free strategy, it can be challenging to achieve, by 2PP-based fabrication techniques, polymeric microresonators with such a small sidewall thickness that still preserve their structural integrity.

Experimental

Femtosecond laser writing

The microstructures were fabricated using a negative-tone photoresist composed of two acrylate monomers and a photoinitiator.[36] The monomers dipentaerythritol pentaacrylate (SR399 – Sartomer®) and tris(2-hydroxy ethyl)isocyanurate tryacrylate (SR368 – Sartomer®) are mixed in a proportion of 90/10 wt%. As photoinitiator we used the 2,4,6-trimethylbenzoyl phenyl phosphinate (in excess of 3 wt%, Irgacure®). Graphene Oxide (GO) (Sigma Aldrich®, powder, 15–20 sheets, 4–10% edge-oxidized) was ultrasonicated for 1 h in 20 mL of ethanol and incorporated into the photoresist in a concentration of 0.0025 wt% (excess weight). The suspension was stirred for 24 h and left to rest until complete evaporation of the solvent (extra 24 hours). It has been shown that the combination of stirring with ultrasonication can reduce the lateral size of GO sheets to a few microns through tensile stress buildup created by drag forces during intense fluid motion[37] and through the formation of C–O groups over the carbon network, which severely weakens the bond energy between carbon atoms.[38] Therefore, the GO in the photoresist probably have a few microns of lateral size. This certainly leads to significant scattering losses, which, along with absorption losses, contribute to the attenuation coefficient measured for the GO-doped polymer.

The fabrication methodology for the GO-doped microresonators followed the description presented in ref. 29.[29] The femtosecond laser writing setup uses a mode-locked Ti:sapphire oscillator (100 fs pulses at 86 MHz repetition rate) operating at 780 nm as the excitation source. The laser beam is focused into the photoresist using a NA 0.25 objective lens. 3D microfabrication is performed by controlling both a galvanometric-mirror system and the stage that supports the sample with a computer-aided software. It is important to mention that we have used the photoresist with the highest concentration of GO before scattering starts to impair the laser writing process. For example, the microstructures fabricated from a photoresist with GO concentration of 0.005 wt% exhibit several structural defects, which hinder their potential as optical resonators. On the other hand, a lower concentration of GO in the photoresist would produce a more subtle mode cleaning effect in the microresonator's resonance spectrum, which is not desirable.

Light coupling

The microresonator modes were characterized by a coupling setup based on evanescent field from a tapered optical fiber.[39] In this setup, we used a broadband source (superluminescent diode) centered at 1.53 μm as the excitation source. The polarization state of light is adjusted by using an in-line polarizer and manual fiber polarization controllers. Light at certain frequencies is coupled to the microresonator using a 2 μm-waist tapered fiber. To properly align the taper and the microresonator, the former is placed in a 3-axis translational stage while the latter is attached to a goniometer placed on a fixed platform. Their positioning is monitored with the aid of a stereomicroscope and a CCD camera. The transmitted light is measured with a 20 pm-resolution optical spectral analyzer (OSA). The WGMs are identified as attenuation peaks in the transmission spectrum.

Absorbance measurements

The absorbance of the pure and the GO-doped polymer material around 1550 nm was analyzed by a Fourier Transform Infrared Spectrophotometer (IRTracer-100). The attenuation coefficient of the undoped (α_p) and the GO-doped acrylate polymer (α_{GO}) was obtained by carrying out absorbance measurements with macroscopic samples with the same composition as those of the microresonators. They are UV-cured freestanding disks with 1.1 mm of thickness and 2 cm of diameter made from both photoresists. By averaging the absorbance measurements taken from different spots of the undoped and GO-doped sample and modeling them with the Beer–Lambert equation, we have found the attenuation coefficient of the undoped and GO-doped polymer to be $\alpha_p = (0.32 \pm 0.05)\ cm^{-1}$ and $\alpha_{GO} = (0.8 \pm 0.1)\ cm^{-1}$ (3.5 dB cm^{-1}) around 1530 nm, respectively.

Conclusions

In conclusion, we investigated the mechanisms behind the mode cleaning observed in GO-doped WGM polymeric microresonators fabricated in a single step of femtosecond laser writing *via* two-photon polymerization. Our results show that the mode cleaning occurs for both polarizations, which renders the influence of polarization-selective effects unlikely. Even though the presence of GO brings up extra losses to the microresonator, the *Q*-factor of the highest extinction ratio resonances does not drop significantly. On the other hand, the low extinction ratio resonances undergo a stronger linewidth broadening and are considerably attenuated. A comparison between the simulated and experimental GO-doped microresonator spectra revealed that the major contribution to the mode cleaning arises

from linear absorption and scattering introduced by GO, though the presence of GO agglomerates inside the microresonator might also be playing a role in filtering some higher-order WGMs out. Finally, the intracavity intensity achieved in the GO-doped microresonators for a pump power on the miliwatt level was found to be several orders of magnitude lower than the saturation intensity of the GO-doped polymer, which rules out completely the contribution of nonlinear absorption to the mode filtering process. Overall, this work offers interesting physical insights that can be useful to the design and fabrication of GO-based photonic micro/nanodevices. For example, the mode cleaning strategy presented herein can be helpful to applications that rely on the resonance shift as a sensing mechanism.

Conflicts of interest

There are no conflicts to declare.

Acknowledgements

The authors gratefully acknowledge financial support from CNPq, São Paulo Research Foundation (FAPESP): grants 2018/11283-7 and 2015/22392-3, CAPES: grant 88882.328716/2018-01 and European Union, project iPhoto-Bio (Ref.: PIRSES-GA-2013-612267).

References

1 F. Bonaccorso, Z. Sun, T. Hasan and A. C. Ferrari, *Nat. Photonics*, 2010, **4**, 611–622.
2 T. Rattana, S. Chaiyakun, N. Witit-anun, N. Nuntawong, P. Chindaudom, S. Oaew, C. Kedkeaw and P. Limsuwan, *ISEEC*, 2012, **32**, 759–764.
3 X. R. Zheng, B. H. Jia, X. Chen and M. Gu, *Adv. Mater.*, 2014, **26**, 2699–2703.
4 X. F. Jiang, L. Polavarapu, S. T. Neo, T. Venkatesan and Q. H. Xu, *J. Phys. Chem. Lett.*, 2012, **3**, 785–790.
5 K. P. Loh, Q. L. Bao, G. Eda and M. Chhowalla, *Nat. Chem.*, 2010, **2**, 1015–1024.
6 S. Stankovich, D. A. Dikin, G. H. B. Dommett, K. M. Kohlhaas, E. J. Zimney, E. A. Stach, R. D. Piner, S. T. Nguyen and R. S. Ruoff, *Nature*, 2006, **442**, 282–286.
7 Q. L. Bao, H. Zhang, J. X. Yang, S. Wang, D. Y. Tong, R. Jose, S. Ramakrishna, C. T. Lim and K. P. Loh, *Adv. Funct. Mater.*, 2010, **20**, 782–791.
8 X. H. Li, K. Wu, Z. P. Sun, B. Meng, Y. G. Wang, Y. S. Wang, X. C. Yu, X. Yu, Y. Zhang, P. P. Shum and Q. J. Wang, *Sci. Rep.*, 2016, **6**, 25266.
9 J. Y. Wu, Y. Y. Yang, Y. Qu, X. Y. Xu, Y. Liang, S. T. Chu, B. E. Little, R. Morandotti, B. H. Jia and D. J. Moss, *Laser Photonics Rev.*, 2019, **13**, 1900056.
10 X. P. Li, Q. M. Zhang, X. Chen and M. Gu, *Sci. Rep.*, 2013, **3**, 1–4.
11 G. C. Righini, Y. Dumeige, P. Feron, M. Ferrari, G. N. Conti, D. Ristic and S. Soria, *Riv. Nuovo Cimento Soc. Ital. Fis.*, 2011, **34**, 435–488.
12 J. Ward and O. Benson, *Laser Photonics Rev.*, 2011, **5**, 553–570.
13 T. A. Ibrahim, R. Grover, L. C. Kuo, S. Kanakaraju, L. C. Calhoun and P. T. Ho, *IEEE Photonics Technol. Lett.*, 2003, **15**, 1422–1424.
14 F. Vollmer, S. Arnold and D. Keng, *Proc. Natl. Acad. Sci. U. S. A.*, 2008, **105**, 20701–20704.
15 D. Venkatakrishnarao, E. A. Mamonov, T. V. Murzina and R. Chandrasekar, *Adv. Opt. Mater.*, 2018, **6**, 1800343.
16 Y. Narayana, D. Venkatakrishnarao, A. Biswas, M. A. Mohiddon, N. Viswanathan and R. Chandrasekar, *ACS Appl. Mater. Interfaces*, 2016, **8**, 952–958.
17 U. Venkataramudu, D. Venkatakrishnarao, N. Chandrasekhar, M. A. Mohiddon and R. Chandrasekar, *Phys. Chem. Chem. Phys.*, 2016, **18**, 15528–15533.
18 B. Sharma, R. R. Frontiera, A. I. Henry, E. Ringe and R. P. Van Duyne, *Mater. Today*, 2012, **15**, 16–25.
19 J. H. An, W. A. El-Said, C. H. Yea, T. H. Kim and J. W. Choi, *J. Nanosci. Nanotechnol.*, 2011, **11**, 4424–4429.
20 A. M. Mohs, M. C. Mancini, S. Singhal, J. M. Provenzale, B. Leyland-Jones, M. D. Wang and S. M. Nie, *Anal. Chem.*, 2010, **82**, 9058–9065.
21 Y. W. Zhu, S. Murali, W. W. Cai, X. S. Li, J. W. Suk, J. R. Potts and R. S. Ruoff, *Adv. Mater.*, 2010, **22**, 3906–3924.
22 G. Eda and M. Chhowalla, *Adv. Mater.*, 2010, **22**, 2392–2415.
23 N. B. Colthup, L. H. Daly and S. E. Wiberley, *Introduction to Infrared and Raman Spectroscopy*, Academic Press, 3rd edn, 1990.
24 O. I. Avila, N. B. Tomazio, A. J. G. Otuka, J. C. Stefanelo, M. B. Andrade, D. T. Balogh and C. R. Mendonca, *J. Polym. Sci., Part B: Polym. Phys.*, 2018, **56**, 479–483.
25 D. S. Correa, P. Tayalia, G. Cosendey, D. S. dos Santos, R. F. Aroca, E. Mazur and C. R. Mendonca, *J. Nanosci. Nanotechnol.*, 2009, **9**, 5845–5849.
26 L. J. Jiang, Y. S. Zhou, W. Xiong, Y. Gao, X. Huang, L. Jiang, T. Baldacchini, J. F. Silvain and Y. F. Lu, *Opt. Lett.*, 2014, **39**, 3034–3037.
27 T. Baldacchini, M. Zimmerley, C. H. Kuo, E. O. Potma and R. Zadoyan, *J. Phys. Chem. B*, 2009, **113**, 12663–12668.
28 A. L. Stancik and E. B. Brauns, *Vib. Spectrosc.*, 2008, **47**, 66–69.
29 N. B. Tomazio, A. J. G. Otuka, G. F. B. Almeida, X. Rosello-Mecho, M. V. Andres and C. R. Mendonca, *J. Polym. Sci., Part B: Polym. Phys.*, 2017, **55**, 569–574.
30 C. R. Pollock and M. Lipson, *Integrated photonics*, Springer Science + Business Media, 2003.
31 E. Garmire, *IEEE J. Sel. Top. Quantum Electron.*, 2000, **6**, 1094–1110.
32 N. B. Tomazio, F. R. Henrique, K. T. Paula, R. D. Fonseca and C. R. Mendonca, SBFOTON International Optics and Photonics Conference, 2019, 1–4.
33 L. N. He, S. K. Ozdemir and L. Yang, *Laser Photonics Rev.*, 2013, **7**, 60–82.
34 V. Zamora, A. Diez, M. V. Andres and B. Gimeno, *Opt. Express*, 2007, **15**, 12011–12016.

35 A. L. Martin, D. K. Armani, L. Yang and K. J. Vahala, *Opt. Lett.*, 2004, **29**, 533–535.
36 T. Baldacchini, C. N. LaFratta, R. A. Farrer, M. C. Teich, B. E. A. Saleh, M. J. Naughton and J. T. Fourkas, *J. Appl. Phys.*, 2004, **95**, 6072–6076.
37 S. Y. Pan and I. A. Aksay, *ACS Nano*, 2011, **5**, 4073–4083.
38 X. D. Qi, T. N. Zhou, S. Deng, G. Y. Zong, X. L. Yao and Q. Fu, *J. Mater. Sci.*, 2014, **49**, 1785–1793.
39 J. C. Knight, G. Cheung, F. Jacques and T. A. Birks, *Opt. Lett.*, 1997, **22**, 1129–1131.